HHS Public Access

Author manuscript

Circ Arrhythm Electrophysiol. Author manuscript; available in PMC 2025 January 01.

Published in final edited form as:

Circ Arrhythm Electrophysiol. 2024 January ; 17(1): e012150. doi:10.1161/CIRCEP.123.012150.

MicroRNA-1 Deficiency is a Primary Etiological Factor Disrupting Cardiac Contractility and Electrophysiological Homeostasis

Dandan Yang, PhD[1], **Xiaoping Wan, PhD**[1], **Neill Schwieterman, BS**[2], **Omer Cavus, MD**[1,5], **Ege Kacira, BS**[1], **Xianyao Xu, MS**[3], **Kenneth R. Laurita, PhD**[4], **Loren E. Wold, PhD**[2], **Thomas J. Hund, PhD**[3], **Peter J. Mohler, PhD**[1], **Isabelle Deschênes, PhD**[1], **Ji-Dong Fu, PhD**[1]

[1]The Dorothy M. Davis Heart and Lung Research Institute, Frick Center for Heart Failure and Arrhythmia, Dept of Physiology and Cell Biology, The Ohio State University, Columbus

[2]The Dorothy M. Davis Heart and Lung Research Institute, Dept of Surgery, Division of Cardiac Surgery, The Ohio State University, Columbus

[3]The Dorothy M. Davis Heart and Lung Research Institute, Frick Center for Heart Failure and Arrhythmia, Depts of Internal Medicine & Biomedical Engineering, The Ohio State University, Columbus

[4]Dept of Medicine, Heart and Vascular Research Center, The MetroHealth System, Case Western Reserve University, Cleveland, OH

[5]Pennsylvania State University, Heart and Vascular Institute, Hershey, PA

Abstract

Background: MicroRNA-1 (miR1), encoded by the genes *miR1-1* and *miR1-2*, is the most abundant miR in the heart and plays a critical role in heart development and physiology. Dysregulation of miR1 has been associated with various heart diseases, where a significant reduction (>75%) in miR1 expression has been observed in patient hearts with atrial fibrillation or acute myocardial infarction. However, it remains uncertain whether miR1-deficiency acts as a primary etiological factor of cardiac remodeling.

Methods: *miR1-1* or *miR1-2* knockout mice were crossbred to produce 75%-miR1-knockdown (75%KD, miR1-1$^{+/-}$:miR1-2$^{-/-}$ or miR1-1$^{-/-}$:miR1-2$^{+/-}$) mice. Cardiac pathology of 75%KD cardiomyocytes/hearts were investigated by echocardiogram, patch clamping, optical mapping, transcriptomic and proteomic assays.

Results: In adult 75%KD hearts, the overall miR1 expression was reduced to ~25% of the normal wildtype (WT) level. These adult 75%KD heart displayed decreased ejection fraction (EF) and fractional shortening (FS), prolonged QRS and QT intervals, and high susceptibility to arrhythmias. Adult 75%KD cardiomyocytes exhibited prolonged action potentials with impaired repolarization and excitation-contraction coupling. Comparatively, 75%KD cardiomyocytes showcased reduced I_{Na} (Na^+ current) and I_{to} (transient outward potassium current), coupled with

Correspondence: Ji-Dong Fu, PhD, The Ohio State University, Graves Hall 5071, 333 W 10th Ave, Columbus, OH 43210, Tel: (614)-685-0657, Jidong.fu@osumc.edu.

Disclosures: None

elevated $I_{Ca,L}$ (L-type Ca^{2+} current), as opposed to WT cells. RNA-sequencing and proteomics assays indicated negative regulation of cardiac muscle contraction and ion channel activities, along with a positive enrichment of smooth muscle contraction genes in 75%KD cardiomyocytes/hearts. miR1 deficiency led to dysregulation of a wide gene network, with miR1's RNAi direct targets influencing many indirectly-regulated genes. Furthermore, after 6 weeks of bi-weekly intravenous tail-vein injection of miR1 mimics, the EF and FS of 75%KD hearts showed significant improvement but remained susceptible to arrhythmias.

Conclusions: miR1 deficiency acts as a primary etiological factor in inducing cardiac remodeling via disrupting heart regulatory homeostasis. Achieving stable and appropriate miR expression levels in the heart is critical for effective miR-based therapy in cardiovascular diseases.

Graphical Abstract

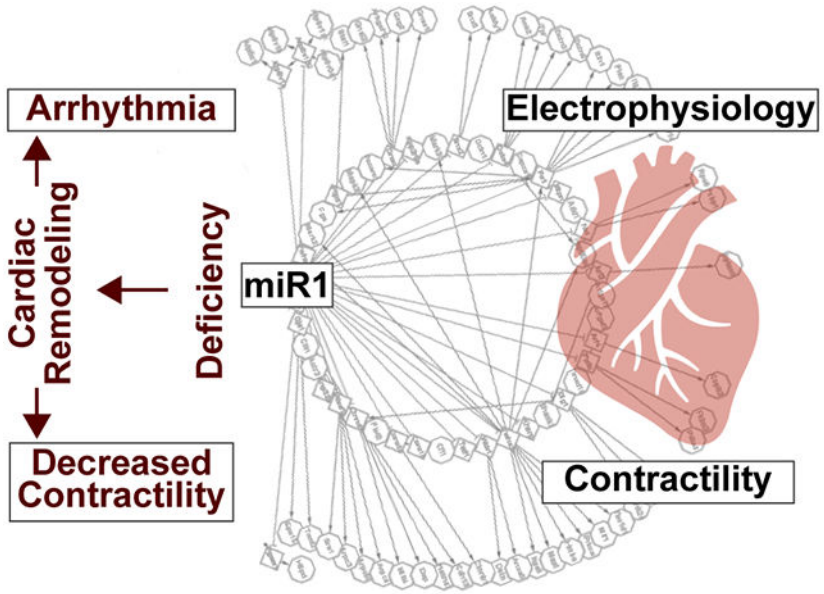

Keywords

microRNA; cardiac remodeling; etiological factor; arrhythmia; contractility

Introduction

Heart disease remains the leading cause of death, imposing a significant health and economic burden on modern society.[1] When faced with environmental and/or genetic changes, the heart undergoes (patho)physiological remodeling adapting to new circulatory demands. Cardiac remodeling encompasses changes in gene expression, molecular, cellular, and interstitial alterations, and clinically presents as modifications in heart size, shape, and function following injury.[2] Cardiomyocytes are the primary cardiac cells involved in this remodeling, alongside the interstitium, fibroblasts, collagen, and coronary vasculature. Patients experiencing major pathological remodeling exhibit a progressive decline in cardiac function, leading to heart failure and malignant ventricular arrhythmias. The molecular mechanisms underlying cardiac remodeling are intricate and involve various genetic

and epigenetic regulatory molecules,[3,4] including microRNAs (miRs).[5] Those regulatory pathways form interconnected molecular networks, making it challenging to elucidate the singular role of any individual factor in the development of cardiac remodeling.

miRs, evolutionarily conserved small non-coding RNA molecules (~22 nucleotides), exert pivotal roles in diverse cellular processes. They finely tune the expression of targeted genes at the posttranscriptional level, and the precise spatiotemporal control of gene expression is critical for maintaining normal heart function. Typically, each miR can directly target hundreds of genes, leading to changes in the expression of thousands of indirectly targeted genes.[6] For instance, miR1, the most abundant miR in the heart, is encoded by two distinct genes, *miR1-1* and *miR1-2*, accounting for approximately 40% of total miR transcripts in the heart.[7] miR1 regulates a wide range of target genes involved in cardiogenesis, intracellular trafficking, cardiac cell cycle, metabolism, cell communication, cardiac excitability, and contractility.[8-12] Studies on *miR1-1* knockout (KO) or *miR1-2* KO mice with 50%-downregulation of miR1 revealed increased susceptibility to perinatal heart failure;[8,10] while complete deletion of miR1 (miR1-1$^{-/-}$:miR1-2$^{-/-}$) resulted in postnatally lethal due to severe cardiac dysfunction.[10,11] The dysregulation of miR1 is implicated in cardiac remodeling in various heart diseases. miR1 is downregulated in murine heart failure model[13,14] and significant decreased (>75%) in hearts of patients with acute myocardial infarction[15] or atrial fibrillation.[16] Conversely, miR1 upregulation in the heart is associated with various types of cardiac arrhythmias as well.[17-20] Notably, upregulation or downregulation of miR1 showed a negative correlation with the expression of cardiac genes directly targeted by miR1, including ion channels, regulatory proteins, and hypertrophy-associated genes. However, it remains unclear whether miR1 deficiency is a primary etiological factor, inducing structure and functional cardiac remodeling and leading to heart failure and malignant arrhythmias, rather than merely being a result of cardiac remodeling.

To investigate the potential etiological role of miR1 deficiency, we generated 75%-miR1-knockdown (75%KD) mice by crossbreeding *miR1-1* KO or *miR1-2* KO transgenic animals. We performed comprehensive assessments of the hemodynamics and electrophysiology of 75%KD hearts. Utilizing a combination of transcriptomic and proteomic analyses alongside functional assays, we examined cardiac cellular function and electrophysiology of 75%KD cardiomyocytes, while also exploring the dysregulation of molecular regulatory networks. Furthermore, we sought to assess if the abnormal functions observed in 75%KD hearts could be rectified by direct *in vivo* administration of miR1. This comprehensive study aimed to shed light on the potential causal role of miR1 deficiency in cardiac dysfunction and to explore possible therapeutic strategies for its modulation.

Methods

Animal models and all experimental procedures have been thoroughly described in the Data Supplement. To ensure ethical and regulatory compliance, the study received institutional review board approval, and all animal studies were conducted following the established institutional guidelines.

Quantification and Statistical Analysis

All biochemistry experiments were independently replicated at least three times. Data are presented as mean±S.E.M, with "n" indicating the number of distinct biological samples. Statistical significance of mean differences was performed using unpaired two-tailed Student's t test, Log-rank (Mantel-Cox) test, or 1-sided Fisher exact test, using GraphPad Prism version 9.4.1 for Windows (GraphPad Software, www.graphpad.com). A $P<0.05$ indicates statistical significance.

Data Availability

The data, methods, and study materials that support the findings of this study are available from the corresponding author upon reasonable request.

Results

The miR1 deficient heart exhibits decreased contractile function and a heightened susceptibility to arrhythmias.

The intercrossing *miR1-1* KO and *miR1-2* KO mice resulted in various genotypes, with 75%KD mice having genotypes of miR1-1$^{+/-}$:miR1-2$^{-/-}$ or miR1-1$^{-/-}$:miR1-2$^{+/-}$. These mice were used to investigate the functional deterioration of adult hearts. We analyzed the genotyping results of special intercrosses in which 50%KD heterozygous (miR1-1$^{+/-}$: miR1-2$^{+/-}$) mice were mated with single-allele 75%KD mice (Fig.1A). A noticeable mortality rate (~10%) was observed among newborns, while no animals with 100%KO genotype survive at the weaning age. However, 50%KD and 75%KD mice survived at the expected Mendelian ratios. Compared to wildtype (WT) animals and 50%KD heterozygous mice, 75%KD mice exhibited a significantly lower survival rate, with unexpected death frequently observed (Fig.1B). We measured the expression level of miR1 in the heart by quantitative RT-PCR (qPCR) and found that the expression of miR1 in the hearts of 75%KD mice was significantly reduced, reaching approximately 25% of the expected level in WT hearts (Fig.1C). Neither the miR1 expression level (S-Fig IA) nor the survival rate showed any significant differences between 75%KD mice with two different genotypes or between male and female animals.

Echocardiography of adult hearts (Fig.1D) showed that 75%KD mice had significantly reduced ejection fraction (EF, 43.946±0.625% [n=8] vs 60.907±0.858% for WT [n=6], $P<0.001$) and fractional shortening (FS, 18.409±0.319% vs. 28.050±0.523% for WT, $P<0.001$) (Fig.1E), indicating severe impairment in hemodynamic function. The left ventricular internal diameter end-systole (LVIDs) was significantly higher in 75%KD mice (3.650±0.0486 mm vs. 3.150±0.050 mm for WT, $P=0.023$), while no significant change was observed in the left ventricular internal diameter end-diastole (LVIDd), suggesting lower ventricular contractility without notable dilation. 75%KD hearts displayed thinner left ventricular posterior walls at both systole (LVPWs, 0.513±0.004 mm vs. 0.733±0.014 mm for WT, $P<0.001$) and diastole (LVPWd, 0.406±0.002 mm vs. 0.467±0.009 mm for WT, $P=0.003$), as well as a thinner interventricular septum at the end of systole (IVSs, 0.525±0.006 mm vs. 0.633±0.009 mm for WT, $P=0.0014$). Surface electrocardiogram measurements (Fig.1F-G) revealed that, under isoflurane anesthesia, the heart rate of

75%KD mice (385±6 bpm, n=9, *P*=0.0436) was significantly slower than that of WT animals (463±11 bpm, n=6). 75%KD mice had significantly prolonged QRS (13.543±0.245 ms, p=0.0147 vs. 10.753±0.199 ms for WT) and QT intervals (35.183±0.334 ms, *P*<0.001 vs. 22.295±0.576 ms for WT) and a shortened PR interval (38.409±0.228 ms, *P*=0.0006 vs. 46.310±0.790 ms for WT). Our surface ECG recording revealed that epinephrine induced premature ventricular contractions, couplets, and non-sustained ventricular tachycardia (NSVT) in 75%KD hearts (2 out of 7 animals) but had no such effect in WT hearts (0 out of 6 mice) (Fig.1H). Consistently, optical mapping assays of *ex vivo* hearts (Fig.1I-J) demonstrated slower propagation of electrical action potential (AP) signals in the ventricle and significantly slower conduction velocity in 75%KD hearts (longitudinal: 0.642±0.010 m/s [n=7], *P*<0.001 vs. 0.755±0.004 m/s [n=10] for WT; transversal: 0.389±0.006 m/s, *P*<0.001 vs. 0.504±0.006 m/s for WT). Additionally, programmed S1-S4 pacing stimulations of ex vivo hearts induced non-sustained ventricular tachycardia frequently in 75%KD hearts (3 out of 8 animals; *P*=0.0491 vs. 0 out of 12 WT animals, Fig.1K-L). Notably, Masson's Trichrome staining didn't reveal significant fibrosis in 75%KD hearts compared to WT tissue (S-Fig IB-C).

In summary, 75%KD mice exhibited cardiac contractile defects and a heightened susceptibility to arrhythmias, suggesting that miR1 deficiency plays an etiological role in inducing significant pathological remodeling in the heart.

miR1 deficiency leads to a broad dysregulation of cardiomyocyte transcriptome.

A large number of genes targeted by miR1 have been reported to be associated with various functions of the heart. Thus, cardiac remodeling resulting from miR1 deficiency can be attributed to the dysregulation of miR1-centered molecular regulatory cascades. To depict the gene regulatory network of miR1, we isolated cardiomyocytes from adult 75%KD and littermate WT mice and performed deep RNA sequencing (RNA-seq, S-Fig IIA). Our analysis revealed that 1,766 genes were differentially expressed in 75%KD cardiomyocytes (fold change >1.5 compared to the WT group, *FDR*<0.05, Fig.2A), including validated miR1 direct targets (e.g., *Slc8a1, Irx5*, *Kcne1*, *Mylk*).

To understand the biological processes primarily affected by miR1 deregulation, we conducted gene ontology (GO) enrichment analysis using ClueGO plugged-in Cytoscape. The enriched biological processes of the differentially-expressed genes were related to cardiac system development, cell-to-cell communication, protein phosphorylation, and ion transports (Fig.2B), aligning with the diverse roles of miR1 in regulating heart development and function maintenance. Further, gene set enrichment analysis (GSEA) of the genome-wide RNA expression revealed a significantly negative normalized enrichment score (NES) for the terms "voltage-gated channel activity" (NES=−2.00, *FDR*< 0.001) (Fig.2C). Analysis of voltage-gated calcium, potassium, and sodium channel genes displayed negative normalized enrichment scores (Fig. 2D-E and S-Fig IIB-C). qPCR analysis validated the significant upregulation of many of miR1's directly targeted genes, including *Kcne1*, *Irx5*, *Slc8a1,* and *B56α*, at the mRNA transcript level in 75%KD myocytes (Fig.2F).

GSEA analysis also revealed a positive involvement of gene expression pattern in smooth muscle contraction in 75%KD myocytes (S-Fig IID), with smooth muscle-specific genes

(e.g., *Acta2*, *Myh11*, *Cnn1*) and miR1-targeted smooth muscle-cell fate controlling factors (e.g., *Myocd, Mylk*, *Dlg1*) being significantly increased. This dysregulation of muscle contractile protein genes may partially explain the decreased hemodynamic function observed in 75%KD hearts (Fig.1). Additionally, gene sets associated with cell fate decision, cell body membrane, and microtube bundle formation were negatively enriched in 75%KD groups, consistent with the positive role of miR1 in regulating cardiogenesis.

In summary, our whole-transcriptome assay demonstrated that miR1 deficiency results in a broad transcriptomic dysregulation of cardiomyocytes. Interestingly, GSEA detected a significant alteration in gene sets involved in cytoplasmic translation, suggesting a disturbance of protein translation in miR1-deficient cells.

The proteomic profile of 75%KD hearts uncovered a complex miR1-driven regulatory network involving multiple interconnected factors.

To gain deeper insights into the cellular and molecular dysfunction in 75%KD hearts at the protein level, we conducted a fractionation mass spectrometry assay on ventricle heart tissues (S-Fig IIIA). This analysis quantified 3,650 proteins from mouse heart tissues, among which the expression of 849 proteins was significantly altered between the two groups. Specifically, 520 proteins were up-regulated, while 329 were down-regulated in 75%KD mice compared to WT (Fig.3A).

GO analysis of the differentially expressed proteins revealed their involvement in broad categories related to heart contraction, cardiac metabolism, cell organization, muscle cell development, and ion channel activities (S-Fig IIIB), largely overlapping with the terms obtained in the RNA-seq analysis. Moreover, GSEA analysis identified that ion channels/transports and cardiac muscle contraction (Fig.3B and S-Fig IIIC) were negatively involved, while smooth muscle contraction and actin filament organization and length regulation were positively involved in 75%KD mice (Fig.3B-C). These findings align with the observed decreased contractile capacity of 75%KD mice. Notably, some miR1 direct targets in cytoskeletal proteins, such as twinfilin-1 (Twf1), myotrophin (Mtpn), and connexin-43 (Cx43), were significantly increased in 75%KD hearts compared with the WT group (Fig.3A). Additionally, cell-to-cell adhesion were positively enriched, and metabolic and mitochondria-related pathways were negatively enriched in 75%KD hearts (S-Fig IIID-E). These results consistently demonstrated that cardiac remodeling in 75%KD hearts was induced by miR1 deficiency. The proteomic profile provided valuable insights into the molecular changes contributing to the observed dysfunction in miR1-deficient hearts.

To explore how miR1 deficiency leads to cardiac remodeling, we examined all miR1 direct targets (729 genes), as predicted by TargetScan[21], in our transcriptome and proteome assays of 75%KD hearts (S-Fig IVA). Among these direct targets, we identified 183 miR1 direct targets that were significantly upregulated in 75%KD cardiomyocytes. Specifically, 126 genes were upregulated at the mRNA transcriptional level, 27 at the protein translational level, and 30 at both mRNA and protein levels. Functional annotation revealed that miR1, through these 183 direct targets, is involved in various biological processes, regulating cardiac electrophysiology, cell morphology, metabolism, and stress responses in the heart (S-Fig IVB). Further analysis with those 57 upregulated miR1 targeted proteins unveiled a

cluster of core genes forming miR1-centered regulatory cascades, which play crucial roles in heart development, electrophysiology, and contraction (Fig.3D). Additionally, using Human Phenotype Ontology, we found that these upregulated miR1 direct target genes are closely associated with a wide range of cardiac diseases (Fig.3E).

Typically, miR dysregulation initiates changes in a small fraction of genes through the RNA interference (RNAi) mechanism, and those miR direct targets could subsequently regulate the expression or activities of large numbers of downstream genes.[22] To better understand the miR1-centered regulatory cascade, we delved into the protein-protein association networks of those 183 miR1 direct targets. This analysis involved in incorporating the proteomic data of proteins that physically or functionally interact with these 183 miR1 targets. Our analysis results in a concise protein-protein interaction network of numerous genes directly or indirectly regulated by miR1 (S-Fig V). The upregulated (red frame) or downregulated (blue frame) component genes of this network illustrate how miR1 deficiency induces remodeling of cardiovascular biological processes via direct targets or indirect protein-protein associations.

Considering that miRs can propagate their regulatory effect through transcription factors,[22-24] we also studied transcription factors that are miR1-targeted genes and were changed in our proteomic study. SP1, a transcription factor, was significantly increased in 75%KD hearts, along with significant changes of a large set of SP1-regulated genes (S-Fig VI). Mapping those SP1-targeted genes, which were upregulated/downregulated in 75%KD hearts, to the functional biological processes, we found their involvement in the regulation of cell communication, transmembrane transport, and cell junction organization. Notably, *Kncd2* is both a miR1 direct target and potentially regulated by SP1, indicating a multi-layer regulatory mechanism of miR1.

Overall, our transcriptomic and proteomic data demonstrated that miR1 deficiency leads to changes in a cluster of directly targeted genes and triggers a large secondary regulatory network, resulting in cardiac remodeling.

The repolarization of AP was impaired in miR1-deficient cardiomyocytes

To assess the functional consequence of miR1 deficiency at the cellular level, we conducted single-cell patch clamping on isolated adult ventricular cardiomyocytes. In 75%KD cardiomyocytes, we observed a significant hyperpolarization of the resting membrane potential (RMP) (−86.729±1.407 mV, n=12, P=0.0438 vs. −77.871±0.480 mV for WT, n=7). The amplitude of APs showed no significant change between 75%KD and WT cells, but the action potential duration (APD) was significantly prolonged (Fig.4A). Specifically, the APD at 50% repolarization (APD50) of 75%KD cells was 20±0.616 ms (P=0.0003 vs. 6.857±0.373 ms for WT) and at 90% repolarization (APD90) was 65.333±2.647 ms (P=0.0402 vs. 36.714±2.166 ms for WT) (Fig.4B). Previous reports have shown that miR1 directly targets multiple voltage-gated ion channels and their accessory proteins.[12] In our voltage clamping experiments, we measured Na^+ current (I_{Na}), L-type Ca^{2+} currents ($I_{Ca,L}$), and transient outward potassium current (I_{to}). Compared to WT cells, 75%KD cardiomyocytes exhibited significantly decreased I_{Na} with a right-shifted voltage dependence of Na^+-channel activation (Fig.4C-E). The half activation voltage (V_{50}) of

Na^+ channels was −18.47±1.82mV in 75%KD cardiomyocytes (n=33, *P*=0.0004 vs. WT −26.25±0.99mV, n=32), while the inactivation curves were the same.

75%KD cardiomyocytes showed a significant increase in $I_{Ca,L}$ particularly at more negative membrane potential voltages (Fig.4F-H). The voltage dependence of Ca^{2+} channels was shifted to the left with a −18.20±1.40 mV V_{50} in 75%KD cells (n=31, *P*<0.0001 vs. WT −7.33±0.91mV, n=34). Although the mRNA expression of the L-type calcium channel α subunit (encoded by *Cacna1c*) was not altered in miR1-deficient hearts, the protein level of β subunit (encoded by *Cacnb2*), known to facilitate the trafficking and enhance the current density of the α subunit,[25-28] was significantly upregulated in 75%KD cardiomyocytes compared to that in WT cells (S-Fig IIIC). Additionally, the I_{to} was significantly smaller in 75%KD cardiomyocytes (4.501±0.100 pA/pF at +30mV, n=22, *P*=0.0001 vs. WT 8.258±0.232 pA/pF, n=12) (Fig.4I). Our whole transcriptome analysis also revealed a specific set of genes correlated with “membrane repolarization” that were significantly negatively enriched in 75%KD hearts (S-Fig VII), including downregulation of *Kcnd2* (S-Fig VIB).

Taken together, our cellular electrophysiological studies demonstrated that miR1 deficiency induces cardiac electrical remodeling, resulting in slower repolarization of APs in 75%KD cardiomyocytes.

Excitation-contraction (E-C) coupling was impaired in miR1-deficient cardiomyocytes

Cardiomyocytes contract in response to electric excitation of the sarcolemma membrane potential depolarization via E-C coupling. To investigate if miR1 deficiency could alter Ca^{2+} handling, we examined the dynamics of intracellular Ca^{2+} transients in 75%KD cardiomyocytes compared to WT cells under basal conditions and in response to isoproterenol (Iso, 100nM) stress (Fig.5A). Under both basal and Iso-stress conditions, the baseline levels of Ca^{2+} transients in 75%KD cardiomyocytes were significantly higher (1.2±0.003, n=59, *P*<0.0001) than that in WT cells (0.935±0.002, n=50, Fig.5B), indicating a Ca^{2+} overload in miR1-deficient cells. However, the amplitudes of Ca^{2+} transients were similar between 75%KD and WT cells (Fig.5C). At the basal state, the upstroke velocity of 75%KD cardiomyocytes was significantly faster (35.212±0.258 vs. 25.48±0.195 for WT, *P*<0.0001) with a reduced time to the peak (Fig.5D-E). The decay time of Ca^{2+} transients was slightly but significantly prolonged in 75%KD myocytes (389.879±1.025 vs. 354.327±1.094 in WT, *P*=0.002, Fig.5G), while the decay rate was similar between the two groups (Fig.5F). Notably, Iso dramatically increased the Ca^{2+} release rate to a similar level in both 75%KD and WT cells, suggesting that the maximum Ca^{2+}-handling capacity of 75%KD cardiomyocytes is comparable to that of WT cells.

The Ca^{2+} store in the sarcoplasmic reticulum (SR) was found to be unchanged, as indicated by the comparable amplitude of caffeine-induced Ca^{2+} release (Fig.5H-K). However, the upstroke velocity of caffeine-induced Ca^{2+} release was significantly faster in 75%KD cells compared to WT cells, indicating faster Ca^{2+} release from the SR. Indeed, the impaired intracellular Ca^{2+} homeostasis is consistent with the discoveries from the omic assays, where changes in many Ca^{2+}-handling genes were detected at the mRNA and/or protein levels (S-Fig VIII).

To further understand the contractile function of 75%KD cardiomyocytes, we studied sarcomere shortening/relaxation with different pacing rates (Fig.6A). At 1 Hz and 3 Hz stimulations, both 75%KD and WT cardiomyocytes demonstrated similar sarcomere shortening with no significant changes in amplitude or percentage shortening rate between these two groups (Fig.6B-C). At 1 Hz pacing, 75%KD myocytes exhibited longer systole and diastole time than WT cells (Fig. 6D-E). At the fast 5 Hz pacing rate that is close to mouse fast heart rate (~500–700 bpm), sarcomere shortening was significantly decreased in 75%KD cells compared to WT cells, with significantly decreased systolic and diastolic velocities (Fig.6F-G), indicating a defect in contractility at higher heart rates.

Transmission electron microscopy of ventricular tissues revealed structure differences in 75%KD cardiomyocytes compared to WT cells. The myofibrils of 75%KD cardiomyocytes were not aligned in parallel, and mitochondria were unevenly positioned among the myofibrils (Fig.6H). Adherens junctions between neighboring 75%KD cardiomyocytes were also more abundant, consistent with the transcriptomic and proteomic findings of positive enrichments in genes associated with cell-cell adhesion/communication in miR1-deficient myocytes.

In summary, miR1 deficiency was found to impair intracellular Ca^{2+} homeostasis and E-C coupling in cardiomyocytes, leading to decreased contractility, particularly at higher pacing rates.

Restoration of miR1 mitigates the contractile deterioration in miR1-deficient hearts.

The comprehensive omics and functional studies conducted in this research revealed that miR1 deficiency plays a critical role as a primary factor in triggering dysfunctions of broad molecular networks in the heart. We next explored the therapeutic potential of restoring miR1 in mitigating the pathological phenotypes observed in miR1-deficient hearts. Paired adult 75%KD mice were selected at 3 months of age and subjected to bi-weekly tail vein injections of Polyethylenimine (PEI)-encapsulated miR1 mimics or control mimics. We monitored the cardiac function by echocardiogram and evaluated the susceptibility to arrhythmia by optical mapping of *ex vivo* hearts (Fig. 7A).

The qRT-PCR assays demonstrated that the miR1 expression level in the heart significantly increased (~2 fold) after three rounds of miR tail-vein injection (Fig. 7B). However, at week 5 post-miR1 delivery, there was no noticeable functional improvement observed in 75%KD hearts. We then extended bi-weekly administration of miR1 and found that, compared to the control mimic group, the hemodynamic function of the heart, including the EF and FS, significantly improved in miR1-administrated animals at week 7 and week 11 post-miR1 delivery (Fig. 7C-D). Relative to the control-mimic group, miR1-mimic treated hearts exhibited lower expression levels of *Myh7* and *Cacna1c*, with no significant changes observed in other examined genes (S-Fig IX). However, it is essential to note that this miR1 treatment didn’t improve the electrical conduction of the ventricle in 75%KD mice (Fig. 7E). Despite the improvement in cardiac contractility, miR1-administrated animals still exhibited a high inducibility to arrhythmias (Fig. 7F). In summary, these results suggest that miR1 restoration has the potential to ameliorate the contractility dysfunction in miR1-deficient

hearts; however, it doesn't fully rescue the arrhythmic susceptibility associated with miR1 deficiency.

Discussion

In the present study, we leveraged miR1-75%KD mice to probe the etiological significance of miR1 in cardiac remodeling. Our findings illuminate how miR1 deficiency alleviates the restraint on its RNAi-direct target genes, subsequently perturbing a comprehensive regulatory gene network and ultimately leading to cardiac remodeling. miR1 deficiency triggers disruptions in cardiac repolarization and E-C coupling within cardiomyocytes, culminating in reduced heart contractility and an increased vulnerability to arrhythmia, ultimately contributing to sudden death in 75%KD mice. A reintroduction of miR1 via tail-vein administration partially reinstated cardiac hemodynamic function, but it proved ineffective in mitigating arrhythmic tendencies, suggesting the intricate balance required for precise miR1 expression within the heart.

miR1 intricately modulates cardiac homeostasis.

In both mice and humans, two discrete genes, *miR1-1* and *miR1-2*, encode mature miR1 with an identical sequence. The expression of miR1 genes progressively increases in muscle cells during the development and maturation of muscle tissues.[29,30] miR1 stands as a predominant miR in the heart, exerting numerous functions crucial for heart homeostasis. Loss-of-function animal models displaying varying degrees of miR1 depletion highlight the sensitivity of miR1 functions to dosage. The survival of adult 75%KD mice indicates that a single allele of either *miR1-1* or *miR1-2* gene is adequate to maintain basal heart function, although an escalated risk of cardiac dysfunction was observed in proportion to the reduction in miR1 levels. While 25%KD mice exhibit no overt cardiac anomalies, those with 50% miR1 reduction generally survive, although some manifest diverse heart developmental irregularities.[8] This study aligns with prior research,[10,11] noting a pre-weaning lethality in miR1-full-KO mice, while 50%KD and 75%KD mice reach adulthood. Although adult 50%KD heterozygous mice display survival rates like WT animals; sudden death emerges in 75%KD mice, implying an aberration in cardiac electrophysiology. Notably, 75%KD adult animals exhibit reduced heart rates, shortened PR intervals extended QT and QRS intervals, along with decreased ventricular conduction velocity (Fig.1).

miR1 orchestrates cardiac electrophysiology by targeting a spectrum of ion channels, transporters, and Ca^{2+} handling proteins.[12] In miR1-deficient 75%KD cardiomyocytes, the expression of several ion channels, including inward rectifier potassium channel Kir2.1 and L-type Ca^{2+} channel subunits, experiences significant upregulation. *Irx5*, known to suppress the expression of *Kcnd2* involved in the I_{to} current, displays elevated level in 75%KD mice, consistent with reduced I_{to} observed in 75%KD cardiomyocytes. Altered I_{to} and enhanced $I_{Ca,L}$ jointly contribute to prolonged APDs in miR1-deficient 75%KD cardiomyocytes. Coupled with the decreased I_{Na} and its right-shifted voltage dependence, this remodeled ion channel profile comprehensively explains the decelerated electrical signal propagation within the ventricle, accompanied by the elongation of both QRS and QT intervals. Beyond ion channel/transport modulation, transmission electron

microscopy reveals structure remodeling in 75%KD cardiomyocytes, characterized by increased adherens junctions. Correspondingly, cardiac remodeling of 75%KD myocytes impacts Ca^{2+} handling and cardiac contractility, evident through Ca^{2+} overload, prolonged decay of Ca^{2+} transients, and reduced cell shortening during fast pacing (5 Hz). At the basal slow pacing rate (1 Hz) and in response to caffeine, notably, 75%KD cardiomyocytes exhibit a faster upstroke velocity of Ca^{2+} transient than WT cells; however, the time-to-peak of cell shortening is prolonged in 75%KD cells, indicating contractile protein remodeling. Our proteomic profiling reveals substantial alterations in the expression of pertinent Ca^{2+} and phosphorylation handling proteins due to miR1 deficiency, encompassing downregulations of Ca^{2+}/calmodulin-dependent protein kinase II γ and δ (encoded by *camk2d* and *camk2g*, respectively), sarcoplasmic/endoplasmic reticulum calcium ATPase 2 (SERCA2), troponin T (TnnT2), and upregulations of protein phosphatase PP2A regulatory subunit B56α (encoded by *PPP2R5A*), sodium-calcium exchanger 1 (NCX1, encoded by *Slc8a1*), β subunit of L-type inward Ca^{2+} channel (S-Fig VIII). Notably, miR1 downregulation has been observed in human heart tissue from acute myocardial infarction[15] and the heart of AF patients.[16] Our study of 75%KD cells/hearts unveils the primary etiological significance of miR1 deficiency in driving cardiac remodeling, although the underlying cause of miR1 deficiency in heart diseases remains enigmatic.

miR1 deficiency orchestrates a comprehensive gene network reshaping cardiac remodeling.

As the predominant miR in the heart, miR1 exerts regulatory control over a diverse array of target genes spanning various biological functions, including cytoskeletal dynamics, cell cycle progression, metabolism, and cardiac electrophysiological properties. Our comprehensive omics analysis of 75%KD cardiomyocytes/hearts consistently illuminates the wide-reaching impact of numerous biological processes. miR1, along with its counterpart miR133, collaboratively suppresses smooth muscle gene expression in the heart. Full-knockout miR1 reactivates smooth muscle genes ectopically in miR1-full-KO hearts.[10] Consistently, our findings also reveal that adult 75%KD hearts prominently express a repertoire of smooth muscle genes (S-Fig IID), such as *Myh11* and *Mylk*, while exhibiting a decreased representation of cardiac muscle genes. The intricate landscape of metabolic and mitochondria-related pathways is also perturbed significantly in 75%KD hearts, as indicated by negative enrichment of terms associated with “inner mitochondrial membrane protein complex” and “oxidative phosphorylation”. This comprehensive transcriptome blueprint of multiple miR1-targeted genes is consistent not only with the disrupted sarcomere organization and diminished cardiac contractility observed in 75%KD mouse cardiomyocytes and hearts (Fig.6), but also with the heightened susceptibility to arrhythmias (Fig.1H, 1J). GSEA analyses of our RNA-seq and proteomic data unveil the downregulation of ion channel/transport terms, including voltage-gated Na^{+}/Ca^{2+}/K^{+} channels, thereby providing mechanistic insights into the prolonged APD (Fig.4) and extended QRS/QT intervals, as well as the reduced conduction velocity of 75%KD hearts (Fig.1G, 1I). Furthermore, a subset of miR1 target proteins, including Twf1, Mtpn, Cx43, and WD-repeat protein 1 (Wdr1), is significantly elevated in 75%KD groups relative to WT. Notably, Twf1 participates as an actin-depolymerizing factor through sequestering actin monomer and capping barbed ends;[31-33] Mtpn is implicated in actin filament growth regulation

and the F-actin-capping protein complex modulation,[34,35] while Wdr1 is known as actin-interacting protein 1 and strongly enhances actin filament disassembly.[36] The influence of miR1 deficiency extends to cytoskeletal regulatory proteins, fostering cardiac remodeling of cell adhesion. Indeed, 75%KD myocytes exhibit augmented adherens junctions in contrast to WT tissues, potentially contributing to increased arrhythmogenic susceptibility, given the pivotal role of gap junctions and adherens junctions in cardiac electromechanical function.[37,38]

At its core, cardiac remodeling in the context of miR1 deficiency is driven by the abrogation of miR1's RNAi actions. A substantial cluster of miR1's RNAi direct target genes, spanning diverse biological themes, demonstrates significant upregulation in 75%KD mice (S-Fig IV). The cardiac anomalies observed in 75%KD heart result from a spatiotemporal convergence of perturbation across multiple biological domains. It is noteworthy that miR1-targeted transcription factor *SP1* displays upregulation in 75%KD hearts, triggering alterations in genes harboring SP1 binding sites, with ensuing impacts on both upregulated or downregulated gene expression (Fig. 3F), reflecting the dual regulatory role of transcription factors in gene modulation.[39] Additionally, proteins often execute their functions through interactions with other proteins or nucleotides (DNA, RNA).[40] miR1's potential to amplify its regulatory impact through protein-to-protein interactions is exemplified in S-Fig V, where miR1's RNAi targets exhibit extensive associations with proteins, many of which undergo differential expression in 75%KD mice. Our annotation reveals the vast repertoire of functionally relevant genes influenced by miR1 deficiency, mirroring the concurrent dysregulation of associated biological processes. While further investigations are required to meticulously map these intricate molecular networks, our findings underscore the pivotal role of miR1 in orchestrating a finely tuned cardiac homeostasis.

Challenges and considerations in harnessing miR1 for therapeutic interventions

Our investigation has underscored the pivotal etiological significance of miR1 deficiency in instigating cardiac remodeling and fostering hemodynamic anomalies and arrhythmias. Unveiling the therapeutic potential of miR1 administration, however, presents a complex landscape. While studies have indicated that miR1 overexpression can enhance the maturation of human stem cell-differentiated cardiomyocytes and hold promise for epigenetic induced-cardiomyocytes,[30,41,42] the multifaceted regulatory nature of miR1 in the heart poses challenges for translating this knowledge into effective cardiovascular therapies. In our bi-weekly administration of miR1-mimics to 75%KD mice via tail-vein injection, we observed limited functional improvement in heart performance only after several weeks of treatment. The restoration of miR1 indeed mitigated the contractile decline in adult miR1-deficient hearts, consistent with prior findings that miR1 reintroduction partially ameliorates sarcomere disruption of neonatal cardiomyocytes lacking miR1.[10] However, the arrhythmia susceptibility of 75%KD hearts remained unaltered despite miR1 administration. One limitation is that sustained VT was not induced in any of those *ex vivo* hearts; programed electrical stimulation performed *in vivo*[43,44] might be able to reveal more severe sustained VT and/or demonstrate miR1's therapeutic potential more comprehensively.

Several factors contribute to these observations. Firstly, rectifying the accumulated cardiac defects spanning fetal to adult stages proves challenging. Additionally, the meticulous control of miR delivery dosage and efficacy presents a formidable hurdle in miR-based gene therapy. Our bi-weekly tail-vein injections achieved a modest two-fold elevation of miR1 expression in 75%KD hearts, which still fell short of normal levels. Furthermore, an excess of miR1 may not necessarily confer greater benefits to the heart. Research has shown that miR1 upregulation post-acute myocardial infarction can exacerbate arrhythmogenesis.[17,45,46] Recent insights have illuminated the multifaceted role of miR1 in regulating cardiac ion channels through a spectrum of mechanisms. Beyond its canonical RNAi pathway, miR1 engages in the modulation of cardiac ion channels by directly binding to ion channel proteins, thereby influencing their activites.[12,47] The administration of miR1-mimics via bi-weekly tail-vein injections may contribute to fluctuations in miR1 expression over time. Such dynamic dosing profiles could disrupt cardiac ion channel functions not only through RNAi-mediated effects but also via intricate biophysical interactions. These multifarious interactions between miR1 and ion channels could collectively contribute to the potential emergence of arrhythmic events. Considering these complexities, achieving a delicate balance in miR1 expression and activity becomes pivotal to the successful implementation of miR-based therapeutic strategies.

Supplementary Material

Refer to Web version on PubMed Central for supplementary material.

Acknowledgments:

The authors are grateful to Dr. Jill Dunham for editorial assistance and thank Dr. Deepak Srivastava for generously sharing miR1-1 homozygous–null (miR1-1$^{-/-}$:miR1-2$^{+/+}$) and miR1-2 homozygous–null (miR1-1$^{+/+}$:miR1-2$^{-/-}$) mice.

Sources of Funding:

This research was supported by the Start-up Fund from the Ohio State University (to J.D.F), funding provided by the OSU President's Research Excellence Accelerator grant (to J.D.F), College of Medicine Office of Research Dean's Nationwide/COM Cross-Campus-Collaborative Pilot Program (to, J.D.F.), grants from the National Institutes of Health (grants NIH-R01HL139006 to I.D. and J.D.F., R21OD031965 to J.D.F, R01HL096962 and R01HL132520 to I.D., R01HL142754 to K.R.L., R01HL139348 and R01AG057046 to L.E.W., R01HL156652 to T.J. H., R01HL135754 to P.J.M.), the CDC/NIOSH (U01 OH012056 to L.E.W.), the Leducq Foundation (TNE FANTASY 19CV03 to P.J.M.), and the American Heart Association (20YVNR35490079 to L.E.W. and P.J.M.). D.Y was funded by the Kenneth M. Rosen Fellowship from the Heart Rhythm Society.

Nonstandard Abbreviations and Acronyms

WT	wildtype
EF	ejection fraction
AP	action potential
APD	action potential duration
APD_{50}	APD at 50% repolarization
APD_{90}	APD at 90% repolarization

Cx43	connexin-43
E-C coupling	Excitation-contraction coupling
FS	fractional shortening
GO	gene ontology
GSEA	gene set enrichment analysis
$I_{Ca,L}$	L-type Ca2+ currents
I_{Na}	Na+ current
Iso	isoproterenol
Ito	transient outward potassium current
IVSd	interventricular septal thickness at the end of diastole
IVSs	interventricular septal thickness at the end of systole
KD	knockdown
KO	knockout
LVIDd	left ventricular internal diameter end-diastole
LVIDs	left ventricular internal diameter end-systole
LVPWd	left ventricular posterior walls at diastole
LVPWs	left ventricular posterior walls at systole
miR	microRNA
Mtpn	myotrophin
NES	normalized enrichment score
NSVT	non-sustained ventricular tachycardia
RMP	resting membrane potential
Twf1	twinfilin-1
V_{50}	half activation voltage

References:

1. Tsao CW, Aday AW, Almarzooq ZI, Alonso A, Beaton AZ, Bittencourt MS, Boehme AK, Buxton AE, Carson AP, Commodore-Mensah Y, et al. Heart disease and stroke statistics-2022 update: A report from the american heart association. Circulation. 2022;145:e153–e639. doi: 10.1161/CIR.0000000000001052 [PubMed: 35078371]
2. Cohn JN, Ferrari R, Sharpe N. Cardiac remodeling--concepts and clinical implications: A consensus paper from an international forum on cardiac remodeling. Behalf of an International Forum on

Cardiac Remodeling. J Am Coll Cardiol. 2000;35:569–582. doi: 10.1016/s0735-1097(99)00630-0 [PubMed: 10716457]

3. Azevedo PS, Polegato BF, Minicucci MF, Paiva SA, Zornoff LA. Cardiac remodeling: Concepts, clinical impact, pathophysiological mechanisms and pharmacologic treatment. Arq Bras Cardiol. 2016;106:62–69. doi: 10.5935/abc.20160005 [PubMed: 26647721]
4. Colpaert R, Calore M. Epigenetics and microRNAs in cardiovascular diseases. Genomics. 2021;113:540–551. doi: 10.1016/j.ygeno.2020.12.042 [PubMed: 33482325]
5. Maries L, Marian C, Sosdean R, Goanta F, Sirbu IO, Anghel A. MicroRNAs-The heart of Post-Myocardial infarction remodeling. Diagnostics (Basel). 2021;11. doi: 10.3390/diagnostics11091675
6. Patel RK, West JD, Jiang Y, Fogarty EA, Grimson A. Robust partitioning of microRNA targets from downstream regulatory changes. Nucleic Acids Res. 2020;48:9724–9746. doi: 10.1093/nar/gkaa687 [PubMed: 32821933]
7. Rao PK, Toyama Y, Chiang HR, Gupta S, Bauer M, Medvid R, Reinhardt F, Liao R, Krieger M, Jaenisch R, et al. Loss of cardiac microRNA-mediated regulation leads to dilated cardiomyopathy and heart failure. Circ Res. 2009;105:585–594. doi: 10.1161/CIRCRESAHA.109.200451 [PubMed: 19679836]
8. Zhao Y, Ransom JF, Li A, Vedantham V, von Drehle M, Muth AN, Tsuchihashi T, Mcmanus MT, Schwartz RJ, Srivastava D. Dysregulation of cardiogenesis, cardiac conduction, and cell cycle in mice lacking miRNA-1-2. Cell. 2007;129:303–317. doi: 10.1016/j.cell.2007.03.030 [PubMed: 17397913]
9. Ivey KN, Srivastava D. MicroRNAs as regulators of differentiation and cell fate decisions. Cell Stem Cell. 2010;7:36–41. doi: 10.1016/j.stem.2010.06.012 [PubMed: 20621048]
10. Heidersbach A, Saxby C, Carver-Moore K, Huang Y, Ang YS, de Jong PJ, Ivey KN, Srivastava D. MicroRNA-1 regulates sarcomere formation and suppresses smooth muscle gene expression in the mammalian heart. Elife. 2013;2:e1323. doi: 10.7554/eLife.01323
11. Wei Y, Peng S, Wu M, Sachidanandam R, Tu Z, Zhang S, Falce C, Sobie EA, Lebeche D, Zhao Y. Multifaceted roles of miR-1s in repressing the fetal gene program in the heart. Cell Res. 2014;24:278–292. doi: 10.1038/cr.2014.12 [PubMed: 24481529]
12. Yang D, Deschenes I, Fu JD. Multilayer control of cardiac electrophysiology by microRNAs. J Mol Cell Cardiol. 2022;166:107–115. doi: 10.1016/j.yjmcc.2022.02.007 [PubMed: 35247375]
13. Ikeda S, He A, Kong SW, Lu J, Bejar R, Bodyak N, Lee KH, Ma Q, Kang PM, Golub TR, et al. MicroRNA-1 negatively regulates expression of the hypertrophy-associated calmodulin and Mef2a genes. Mol Cell Biol. 2009;29:2193–2204. doi: 10.1128/MCB.01222-08 [PubMed: 19188439]
14. Li M, Chen X, Chen L, Chen K, Zhou J, Song J. MiR-1-3p that correlates with left ventricular function of HCM can serve as a potential target and differentiate HCM from DCM. J Transl Med. 2018;16:161. doi: 10.1186/s12967-018-1534-3 [PubMed: 29885652]
15. Pinchi E, Frati P, Aromatario M, Cipolloni L, Fabbri M, La Russa R, Maiese A, Neri M, Santurro A, Scopetti M, et al. MiR-1, miR-499 and miR-208 are sensitive markers to diagnose sudden death due to early acute myocardial infarction. J Cell Mol Med. 2019;23:6005–6016. doi: 10.1111/jcmm.14463 [PubMed: 31240830]
16. Girmatsion Z, Biliczki P, Bonauer A, Wimmer-Greinecker G, Scherer M, Moritz A, Bukowska A, Goette A, Nattel S, Hohnloser SH, et al. Changes in microRNA-1 expression and IK1 up-regulation in human atrial fibrillation. Heart Rhythm. 2009;6:1802–1809. doi: 10.1016/j.hrthm.2009.08.035 [PubMed: 19959133]
17. Yang B, Lin H, Xiao J, Lu Y, Luo X, Li B, Zhang Y, Xu C, Bai Y, Wang H, et al. The muscle-specific microRNA miR-1 regulates cardiac arrhythmogenic potential by targeting GJA1 and KCNJ2. Nat Med. 2007;13:486–491. doi: 10.1038/nm1569 [PubMed: 17401374]
18. Xu HF, Ding YJ, Shen YW, Xue AM, Xu HM, Luo CL, Li BX, Liu YL, Zhao ZQ. MicroRNA-1 represses Cx43 expression in viral myocarditis. Mol Cell Biochem. 2012;362:141–148. doi: 10.1007/s11010-011-1136-3 [PubMed: 22045061]
19. Shan H, Zhang Y, Cai B, Chen X, Fan Y, Yang L, Chen X, Liang H, Zhang Y, Song X, et al. Upregulation of microRNA-1 and microRNA-133 contributes to arsenic-induced cardiac electrical remodeling. Int J Cardiol. 2013;167:2798–2805. doi: 10.1016/j.ijcard.2012.07.009 [PubMed: 22889704]

20. Jia X, Zheng S, Xie X, Zhang Y, Wang W, Wang Z, Zhang Y, Wang J, Gao M, Hou Y. MicroRNA-1 accelerates the shortening of atrial effective refractory period by regulating KCNE1 and KCNB2 expression: An atrial tachypacing rabbit model. Plos One. 2013;8:e85639. doi: 10.1371/journal.pone.0085639 [PubMed: 24386485]
21. Lewis BP, Burge CB, Bartel DP. Conserved seed pairing, often flanked by adenosines, indicates that thousands of human genes are microRNA targets. Cell. 2005;120:15–20. doi: 10.1016/j.cell.2004.12.035 [PubMed: 15652477]
22. Tu K, Yu H, Hua YJ, Li YY, Liu L, Xie L, Li YX. Combinatorial network of primary and secondary microRNA-driven regulatory mechanisms. Nucleic Acids Res. 2009;37:5969–5980. doi: 10.1093/nar/gkp638 [PubMed: 19671526]
23. Rhoades MW, Reinhart BJ, Lim LP, Burge CB, Bartel B, Bartel DP. Prediction of plant microRNA targets. Cell. 2002;110:513–520. doi: 10.1016/s0092-8674(02)00863-2 [PubMed: 12202040]
24. Enright AJ, John B, Gaul U, Tuschl T, Sander C, Marks DS. MicroRNA targets in Drosophila. Genome Biol. 2003;5:R1. doi: 10.1186/gb-2003-5-1-r1 [PubMed: 14709173]
25. De Waard M, Pragnell M, Campbell KP. Ca2+ channel regulation by a conserved beta subunit domain. Neuron. 1994;13:495–503. doi: 10.1016/0896-6273(94)90363-8 [PubMed: 8060623]
26. Pragnell M, De Waard M, Mori Y, Tanabe T, Snutch TP, Campbell KP. Calcium channel beta-subunit binds to a conserved motif in the I-II cytoplasmic linker of the alpha 1-subunit. Nature. 1994;368:67–70. doi: 10.1038/368067a0 [PubMed: 7509046]
27. Chien AJ, Zhao X, Shirokov RE, Puri TS, Chang CF, Sun D, Rios E, Hosey MM. Roles of a membrane-localized beta subunit in the formation and targeting of functional L-type Ca2+ channels. J Biol Chem. 1995;270:30036–30044. doi: 10.1074/jbc.270.50.30036 [PubMed: 8530407]
28. Dalton S, Takahashi SX, Miriyala J, Colecraft HM. A single CaVbeta can reconstitute both trafficking and macroscopic conductance of voltage-dependent calcium channels. J Physiol. 2005;567:757–769. doi: 10.1113/jphysiol.2005.093195 [PubMed: 16020456]
29. Ivey KN, Muth A, Arnold J, King FW, Yeh RF, Fish JE, Hsiao EC, Schwartz RJ, Conklin BR, Bernstein HS, et al. MicroRNA regulation of cell lineages in mouse and human embryonic stem cells. Cell Stem Cell. 2008;2:219–229. doi: 10.1016/j.stem.2008.01.016 [PubMed: 18371447]
30. Fu JD, Rushing SN, Lieu DK, Chan CW, Kong CW, Geng L, Wilson KD, Chiamvimonvat N, Boheler KR, Wu JC, et al. Distinct roles of microRNA-1 and −499 in ventricular specification and functional maturation of human embryonic stem cell-derived cardiomyocytes. Plos One. 2011;6:e27417. doi: 10.1371/journal.pone.0027417 [PubMed: 22110643]
31. Palmgren S, Vartiainen M, Lappalainen P. Twinfilin, a molecular mailman for actin monomers. J Cell Sci. 2002;115:881–886. doi: 10.1242/jcs.115.5.881 [PubMed: 11870207]
32. Moseley JB, Okada K, Balcer HI, Kovar DR, Pollard TD, Goode BL. Twinfilin is an actin-filament-severing protein and promotes rapid turnover of actin structures in vivo. J Cell Sci. 2006;119:1547–1557. doi: 10.1242/jcs.02860 [PubMed: 16569665]
33. Johnston AB, Collins A, Goode BL. High-speed depolymerization at actin filament ends jointly catalysed by Twinfilin and Srv2/CAP. Nat Cell Biol. 2015;17:1504–1511. doi: 10.1038/ncb3252 [PubMed: 26458246]
34. Bhattacharya N, Ghosh S, Sept D, Cooper JA. Binding of myotrophin/V-1 to actin-capping protein: Implications for how capping protein binds to the filament barbed end. J Biol Chem. 2006;281:31021–31030. doi: 10.1074/jbc.M606278200 [PubMed: 16895918]
35. Takeda S, Minakata S, Koike R, Kawahata I, Narita A, Kitazawa M, Ota M, Yamakuni T, Maeda Y, Nitanai Y. Two distinct mechanisms for actin capping protein regulation--steric and allosteric inhibition. Plos Biol. 2010;8:e1000416. doi: 10.1371/journal.pbio.1000416 [PubMed: 20625546]
36. Ono S. Functions of actin-interacting protein 1 (AIP1)/WD repeat protein 1 (WDR1) in actin filament dynamics and cytoskeletal regulation. Biochem Biophys Res Commun. 2018;506:315–322. doi: 10.1016/j.bbrc.2017.10.096 [PubMed: 29056508]
37. Peters NS, Severs NJ, Rothery SM, Lincoln C, Yacoub MH, Green CR. Spatiotemporal relation between gap junctions and fascia adherens junctions during postnatal development of human ventricular myocardium. Circulation. 1994;90:713–725. doi: 10.1161/01.cir.90.2.713 [PubMed: 8044940]

38. Angst BD, Khan LU, Severs NJ, Whitely K, Rothery S, Thompson RP, Magee AI, Gourdie RG. Dissociated spatial patterning of gap junctions and cell adhesion junctions during postnatal differentiation of ventricular myocardium. Circ Res. 1997;80:88–94. doi: 10.1161/01.res.80.1.88 [PubMed: 8978327]

39. Boyle P, Despres C. Dual-function transcription factors and their entourage: Unique and unifying themes governing two pathogenesis-related genes. Plant Signal Behav. 2010;5:629–634. doi: 10.4161/psb.5.6.11570 [PubMed: 20383056]

40. Langley SR, Dwyer J, Drozdov I, Yin X, Mayr M. Proteomics: From single molecules to biological pathways. Cardiovasc Res. 2013;97:612–622. doi: 10.1093/cvr/cvs346 [PubMed: 23180722]

41. Nam YJ, Song K, Luo X, Daniel E, Lambeth K, West K, Hill JA, Dimaio JM, Baker LA, Bassel-Duby R, et al. Reprogramming of human fibroblasts toward a cardiac fate. Proc Natl Acad Sci U S A. 2013;110:5588–5593. doi: 10.1073/pnas.1301019110 [PubMed: 23487791]

42. Bektik E, Dennis A, Prasanna P, Madabhushi A, Fu JD. Single cell qPCR reveals that additional HAND2 and microRNA-1 facilitate the early reprogramming progress of seven-factor-induced human myocytes. Plos One. 2017;12:e183000. doi: 10.1371/journal.pone.0183000

43. Osbourne A, Calway T, Broman M, McSharry S, Earley J, Kim GH. Downregulation of connexin43 by microRNA-130a in cardiomyocytes results in cardiac arrhythmias. J Mol Cell Cardiol. 2014;74:53–63. doi: 10.1016/j.yjmcc.2014.04.024. [PubMed: 24819345]

44. Wang Q, Quick AP, Cao S, Reynolds J, Chiang DY, Beavers D, Li N, Wang G, Rodney GG, Anderson ME, et al. Oxidized CaMKII (Ca2+/Calmodulin-Dependent Protein Kinase II) Is Essential for Ventricular Arrhythmia in a Mouse Model of Duchenne Muscular Dystrophy. Circ Arrhythm Electrophysiol. 2018;11(4):e005682. doi: 10.1161/CIRCEP.117.005682. [PubMed: 29654126]

45. Terentyev D, Belevych AE, Terentyeva R, Martin MM, Malana GE, Kuhn DE, Abdellatif M, Feldman DS, Elton TS, Gyorke S. MiR-1 overexpression enhances Ca(2+) release and promotes cardiac arrhythmogenesis by targeting PP2A regulatory subunit B56alpha and causing CaMKII-dependent hyperphosphorylation of RyR2. Circ Res. 2009;104:514–521. doi: 10.1161/CIRCRESAHA.108.181651 [PubMed: 19131648]

46. Su X, Liang H, Wang H, Chen G, Jiang H, Wu Q, Liu T, Liu Q, Yu T, Gu Y, et al. Over-expression of microRNA-1 causes arrhythmia by disturbing intracellular trafficking system. Sci Rep. 2017;7:46259. doi: 10.1038/srep46259 [PubMed: 28397788]

47. Yang D, Wan X, Dennis AT, Bektik E, Wang Z, Costa M, Fagnen C, Venien-Bryan C, Xu X, Gratz DH, et al. MicroRNA biophysically modulates cardiac action potential by direct binding to ion channel. Circulation. 2021;143:1597–1613. doi: 10.1161/CIRCULATIONAHA.120.050098 [PubMed: 33590773]

48. Cavus O, Williams J, Musa H, El RM, Gratz D, Shaheen R, Schwieterman NA, Koenig S, Antwi-Boasiako S, Young LJ, et al. Giant ankyrin-G regulates cardiac function. J Biol Chem. 2021; 296:100507. doi: 10.1016/j.jbc.2021.100507 [PubMed: 33675749]

49. Tian XL, Yong SL, Wan X, Wu L, Chung MK, Tchou PJ, Rosenbaum DS, Van Wagoner DR, Kirsch GE, Wang Q. Mechanisms by which SCN5A mutation N1325S causes cardiac arrhythmias and sudden death in vivo. Cardiovasc Res. 2004;61:256–267. doi: 10.1016/j.cardiores.2003.11.007 [PubMed: 14736542]

50. Bindea G, Mlecnik B, Hackl H, Charoentong P, Tosolini M, Kirilovsky A, Fridman WH, Pages F, Trajanoski Z, Galon J. ClueGO: A Cytoscape plug-in to decipher functionally grouped gene ontology and pathway annotation networks. Bioinformatics. 2009;25:1091–1093. doi: 10.1093/bioinformatics/btp101 [PubMed: 19237447]

51. Shannon P, Markiel A, Ozier O, Baliga NS, Wang JT, Ramage D, Amin N, Schwikowski B, Ideker T. Cytoscape: A software environment for integrated models of biomolecular interaction networks. Genome Res. 2003; 13:2498–2504. doi: 10.1101/gr.1239303 [PubMed: 14597658]

52. Subramanian A, Tamayo P, Mootha VK, Mukherjee S, Ebert BL, Gillette MA, Paulovich A, Pomeroy SL, Golub TR, Lander ES, et al. Gene set enrichment analysis: A knowledge-based approach for interpreting genome-wide expression profiles. Proc Natl Acad Sci U S A. 2005; 102:15545–15550. doi: 10.1073/pnas.0506580102 [PubMed: 16199517]

53. Mootha VK, Lindgren CM, Eriksson KF, Subramanian A, Sihag S, Lehar J, Puigserver P, Carlsson E, Ridderstrale M, Laurila E, et al. PGC-1alpha-responsive genes involved in oxidative

phosphorylation are coordinately downregulated in human diabetes. Nat Genet. 2003; 34:267–273. doi: 10.1038/ng1180 [PubMed: 12808457]

54. Liberzon A, Subramanian A, Pinchback R, Thorvaldsdottir H, Tamayo P, Mesirov JP. Molecular signatures database (MSigDB) 3.0. Bioinformatics. 2011; 27:1739–1740. doi: 10.1093/bioinformatics/btr260 [PubMed: 21546393]
55. Liberzon A, Birger C, Thorvaldsdottir H, Ghandi M, Mesirov JP, Tamayo P. The Molecular Signatures Database (MSigDB) hallmark gene set collection. Cell Syst. 2015; 1:417–425. doi: 10.1016/j.cels.2015.12.004 [PubMed: 26771021]
56. Szklarczyk D, Franceschini A, Wyder S, Forslund K, Heller D, Huerta-Cepas J, Simonovic M, Roth A, Santos A, Tsafou KP, et al. STRING v10: Protein-protein interaction networks, integrated over the tree of life. Nucleic Acids Res. 2015;43:D447–D452. doi: 10.1093/nar/gku1003 [PubMed: 25352553]

What is Known:

- MicroRNA-1 is the most abundant microRNA in the heart.
- MicroRNA-1 expression is reduced in hearts of patients with atrial fibrillation or acute myocardial infarction.

What the Study Adds:

- Our extensive assessments unveil compromised hemodynamic function and elevated arrhythmogenesis risk in microRNA1-75%-knockdown hearts.
- MicroRNA-1 deficiency disrupts the homeostasis of molecular regulatory gene networks, serving as a primary etiological factor in cardiac remodeling.
- MicroRNA-1 treatment notably improves the contractility of miR1-deficient hearts; however, it fails to alleviate their heightened susceptibility to arrhythmias.

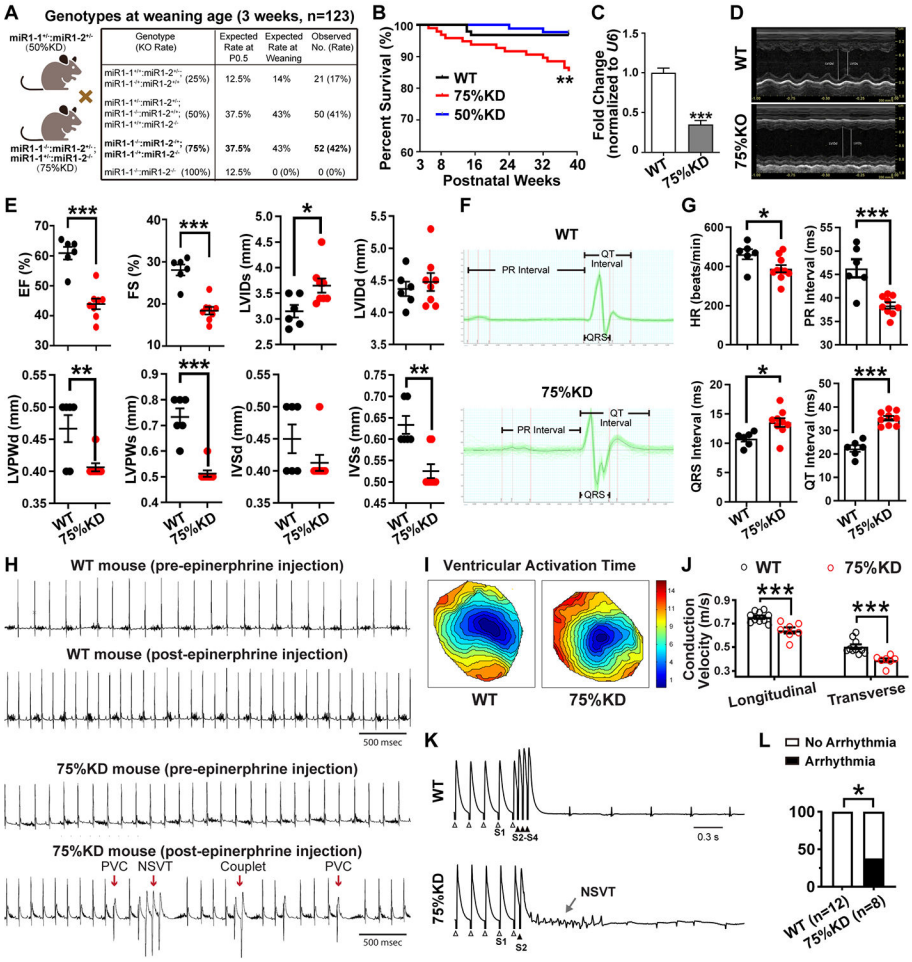

Figure 1.

Cardiac dysfunction and increased ventricular arrhythmia susceptibility in miR1-deficient mice. (**A**) Genotypes of offspring generated from 50% knockdown (50%KD) heterozygous (miR1-1$^{+/-}$: miR1-2$^{+/-}$) mice and single-allele 75%KD (miR1-1$^{+/-}$: miR1-2$^{-/-}$ or miR1-1$^{-/-}$: miR1-2$^{+/-}$) mice intercrosses. Expected genotype ratios were calculated at postnatal day 0.5 (P0.5) and weaning age; animals were genotyped at weaning age. (**B**) Kaplan-Meier survival curve of 50%KD (n=86), 75%KD (n=134), and wild-type (WT, n=84) littermates. (**C**) qPCR analysis showing approximately 70% lower expression level of miR in the heart of adult 75%KD mice (n=10, p<0.001) compared to that in WT mice (n=7). The expression level was normalized to *U6* RNA. (**D-E**) Representative echocardiography images (M-mode, D) and analysis (E) indicating significantly decreased cardiac function in adult 75%KD mice (n=9) compared to WT (n=6). EF, ejection fraction; FS, fractional shortening; LVIDs, left ventricular internal diameter end-systole; LVIDd, left ventricular internal diameter end-diastole; LVPWs, left ventricular posterior wall thickness at the end of systole; LVPWd, left ventricular posterior wall thickness at the end of diastole; IVSs interventricular septal thickness at the end of systole; IVSd, interventricular septal thickness at the end of diastole. (**F-G**) Representative traces of surface electrocardiography (F) and analysis (G) showing reduced heart rate, shortened

PR interval, and prolonged QRS and QT intervals in 75%KD mice (n=8) compared to WT (n=6). (**H**) Surface electrocardiography revealed a high vulnerability of 75%KD mice to arrhythmias, indicated by premature ventricular contractions (PVCs), couplets, and non-sustained ventricular tachycardia (NSVT) induced by epinephrine. (**I-J**) Representative contour map of ventricular activation time (I) in 75%KD and WT hearts during pacing. A summarized bar graph of conduction velocity (J) indicating isochrone crowding and slower action potential propagation in 75%KD hearts (n=7) compared to WT (n=10). (**K-L**) Representative traces of programmed electric stimulation assays of ex vivo hearts (K) and analysis (L) revealing higher arrhythmia inducibility of 75%KD hearts (n=8, p=0.049) compared to WT hearts (n=12). △ and ▲ indicate S1 and S2-S4 stimulations, respectively. *P<0.05, **P<0.01, ***P<0.001 versus WT group. The statistical significance of differences estimated using unpaired two-tailed Student t-tests (panels C, E, G, J), Log-rank (Mantel-Cox) test (panel B), and 1-sided Fisher exact test (panel J).

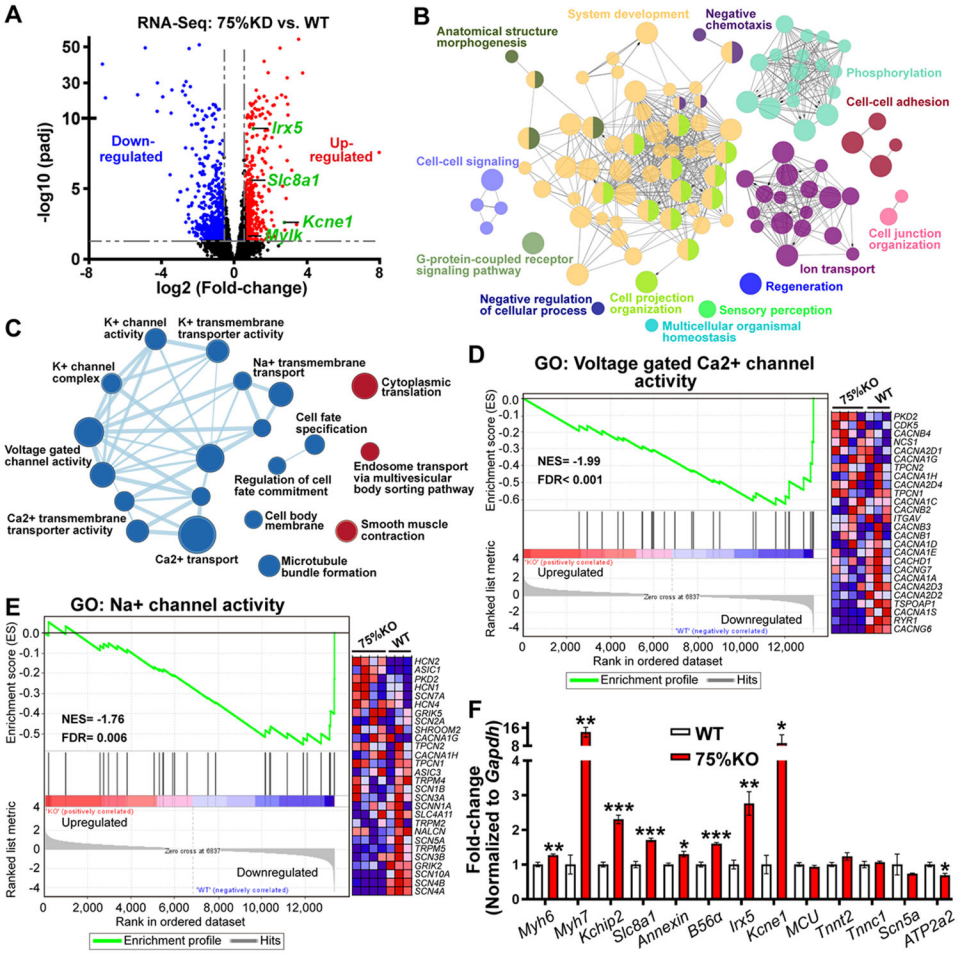

Figure 2.

Reshaping of cardiomyocyte transcription profile by miR1 deficiency. (**A**) Volcano plot displaying expressed RNAs with transcript per million (TPM) >1 in both 75%KD and WT cardiomyocytes. A false discovery rate (*FDR*) of <0.05 is indicative of significant enrichment. Transcripts with log2 fold change ≥1.5 or ≤−1.5 (*FDR*<0.05) are highlighted in red or blue, respectively. Previously validated miR1 direct targets are highlighted in green. (**B**) ClueGO plugged-in Cytoscape analysis presenting differentially-expressed genes between 75%KD and WT myocytes, organized by gene ontology terms. Each bubble (network node) represents a specific biological process or pathway, and lines (network edges) denote relationships between different terms. Nodes of the same color indicate functionally related terms or pathways. Node size represents term enrichment significance (*P*<0.0005 to <0.05). (**C**) Gene set enrichment analysis (GSEA) of transcriptome comparison between 75%KD and WT groups. Normalized enrichment score (NES) indicates negative or positive enrichment in 75%KD cardiomyocytes. An enrichment map of Cytoscape summarizes gene sets related to cardiac electrophysiology. Node size reflects the number of associated genes, and network edges display similarity between different gene sets. Filled node colors indicate positively (red) or negatively (blue) enrichment in 75%KD groups. (**D-E**) Assessment of the regulation of the gene ontology (GO) terms, showing positive regulation of calcium transport into the cytosol (D) and sodium channel

activity (E), accompanied by heatmaps depicting low (blue) to high (red) expression of individual component genes. (**F**) qPCR analysis validating that many of miR1's RNAi direct targets were upregulated at the transcriptional level in 75%KD groups compared to WT. Gene expressions were normalized to the *Gapdh* housekeeping gene. *$P<0.05$, **$P<0.01$, ***$P<0.001$ versus WT group. Statistical significance of differences estimated using analysis of variance followed by unpaired two-tailed Student *t*-tests with multiple testing adjustments.

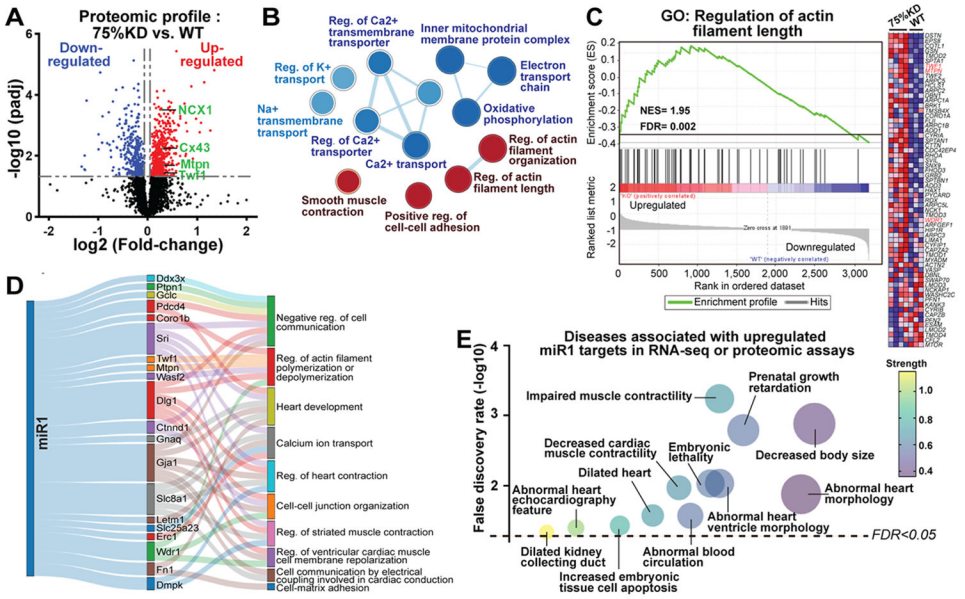

Figure 3.

Revealing the combinatorial regulatory network of miR1 in heart homeostasis. (**A**) Volcano plot displaying the log2 fold change of expressed proteins in 75%KD and WT ventricular tissues, detected by mass spectrometry. Significantly upregulated or downregulated proteins in 75%KD hearts are highlighted in red and blue, respectively. Direct miR1 target proteins are denoted by green text. (**B**) GSEA proteomic comparison of 75%KD and WT mouse hearts revealed a positive enrichment of cardiomyocyte contractile. NES denotes negative or positive enrichments in 75%KD cardiomyocytes. An *FDR* <0.05 is considered a significant enrichment. Node size corresponds to the number of genes, and network edges represent similarity between different gene sets. Filled node colors indicate positively (red) or negatively (blue) enriched gene terms in 75%KD groups. (**C**) Evaluation of the regulation of the GO term revealed positive regulation of actin filament length, alongside heatmaps illustrating low (blue) to high (red) expression of each gene. Cytoskeletal protein names among miR1's direct targets are highlighted in red. (**D**) Sankey diagram based on the Gene Ontology Biological Process (GO_BP) analyses, depicting biological processes, including cardiac electrophysiology and contractile, associated with miR1 target proteins upregulated in 75%KD hearts. (**E**) Human Phenotype Ontology analysis of upregulated miR1 direct targets revealed a diverse array of cardiovascular diseases listed in the OMIM database. Node size represents the number of associated genes.

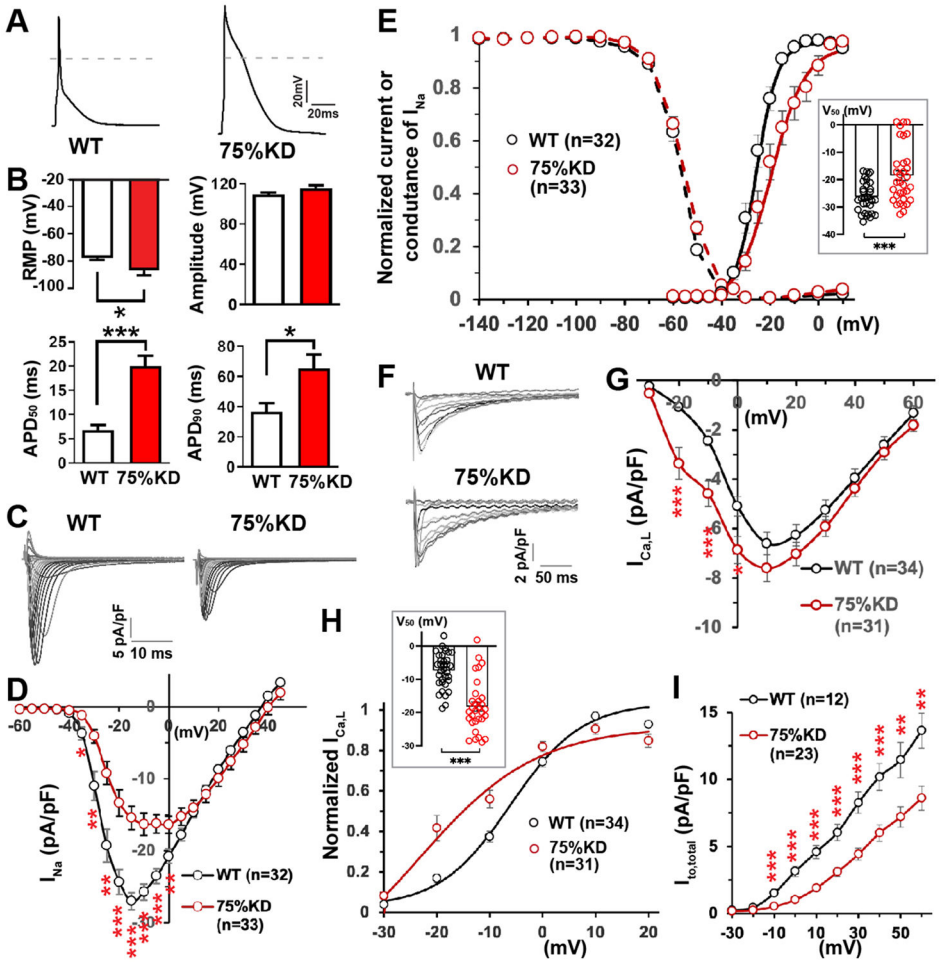

Figure 4.

Altered cellular electrophysiology in miR1-deficient cardiomyocytes. **(A)** Representative action potential (AP) traces from both adult 75%KD and WT ventricular cardiomyocytes. (**B**) Statistical analyses portraying resting membrane potential (RMP), amplitude, and AP duration at 50% (APD_{50}) and 90% (APD_{90}) repolarization of 75%KD (n=12) and WT (n=7) ventricular cardiomyocytes. (**C-E**) Representative traces (C) and I/V curves (D) of Na^+ current (I_{Na}), showcasing diminished I_{Na} in 75%KD cardiomyocytes relative to WT cells. Activation curve (E, solid lines) highlights a right shifted voltage dependence of Na^+-channel activation in 75%KD cardiomyocytes, while inactivation curves (dash lines) show no significant difference between 75%KD and WT cells. Inserted box in panel E provides the summarized half activation voltage (V_{50}). (**F-H**) Representative traces (F), I/V curves (G), and activation curves (H) of L-type Ca^{2+} current ($I_{Ca,\ L}$), indicating earlier activation of $I_{Ca,\ L}$ in 75%KD cardiomyocytes compared to WT cells. Inserted box of panel H presents the summarized V_{50} of $I_{Ca,\ L}$. **(I)** I/V curves of total transient outward potassium current ($I_{to,\ total}$), revealing significantly declined $I_{to,\ total}$ in 75%KD cardiomyocytes relative to WT cells. **P*<0.05, ***P*<0.01, ****P*<0.001 versus WT group. Statistical significance of differences was assessed by unpaired two-tailed Student *t*-tests.

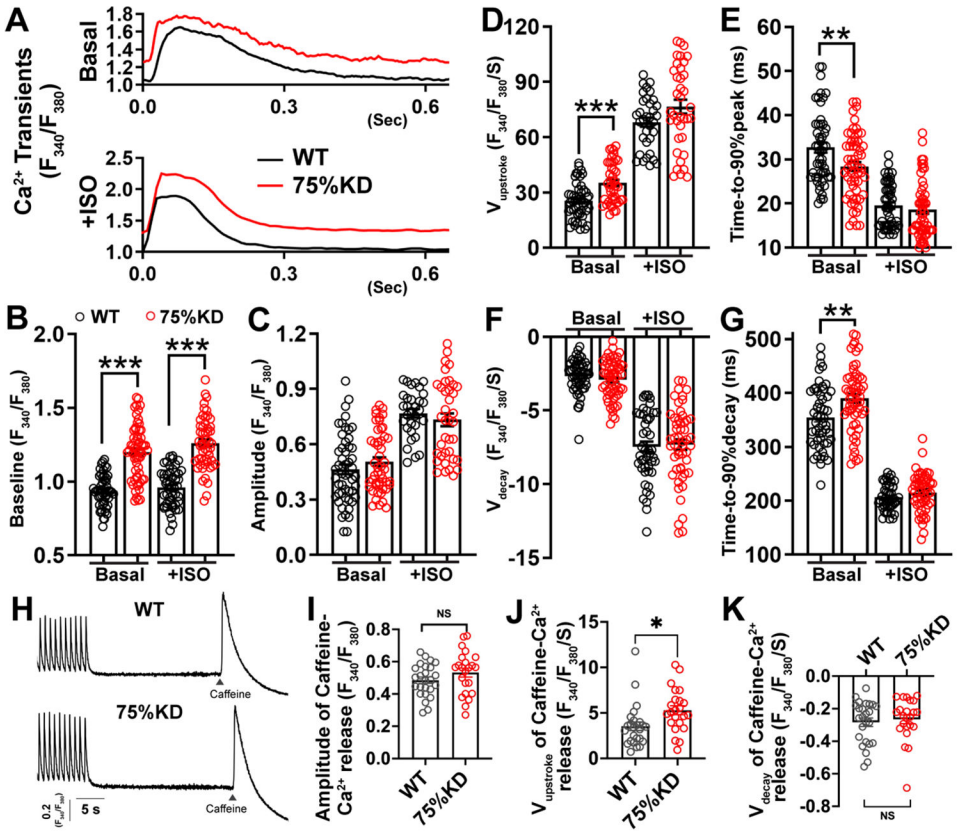

Figure 5.

Impaired intracellular Ca^{2+} handling in 75%KD cardiomyocytes. **(A)** Representative Ca^{2+} transient traces observed in 75%KD and WT ventricular cardiomyocytes under normal (top) and stress induced by isoproterenol treatment (Iso, 100nM) (bottom). (**B-G**) Statistical analyses illustrating Ca^{2+} transient parameters in 75%KD (n=59) and WT (n=50) cardiomyocytes, including intracellular Ca^{2+} baseline level (B), amplitude (C), Ca^{2+} upstroke velocity ($V_{upstroke}$, D), time to 90% of peak (E), Ca^{2+} decay velocity (V_{decay}, F), and time to 90% of baseline (G). (**H-K**) Representative traces (H) of caffeine-induced Ca^{2+} release observed in WT (n=25) and 75%KD (n=23) cardiomyocytes, along with statistical analyses of amplitude (I), $V_{upstroke}$ (J), and V_{decay} (K). ***P*<0.01, ****P*<0.001 versus WT group. Statistical significance of differences was assessed by unpaired two-tailed Student *t*-tests.

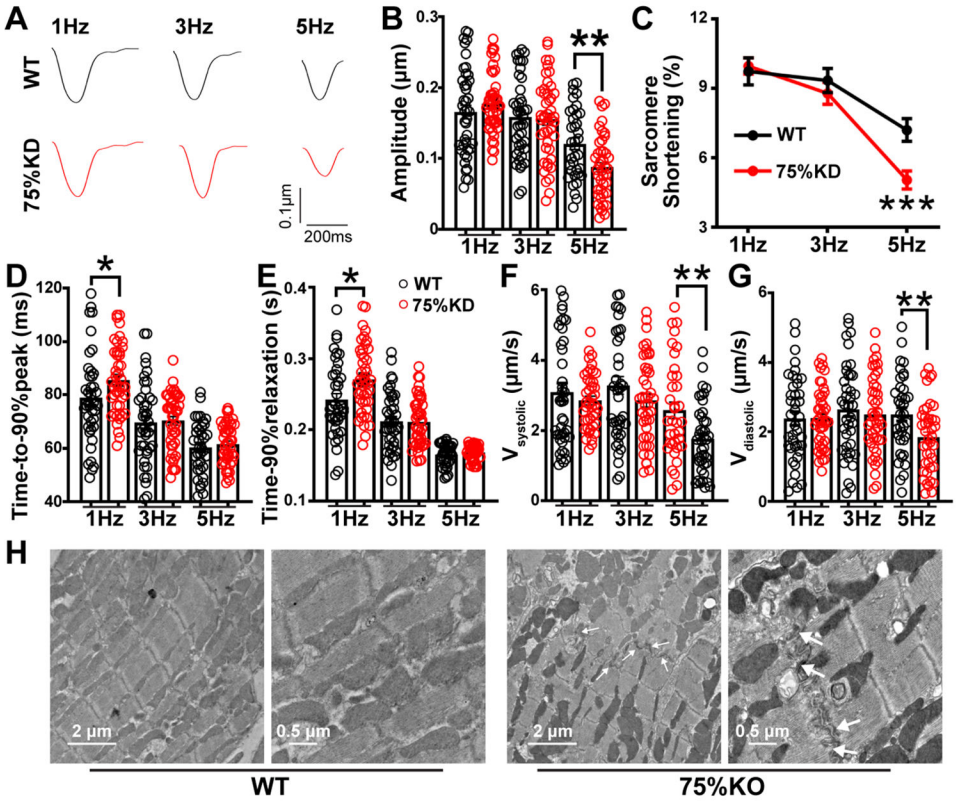

Figure 6.

Contractility defects in miR1-deficient cardiomyocytes. (**A**) Representative sarcomere shortening traces of 75%KD (n=49) and WT (n=50) cardiomyocytes paced at rates of 1Hz, 3Hz, or 5Hz. (**B-G**) Statistical analyses of sarcomere shortening parameters, including amplitude (B), percentile of sarcomere shortening (C), time from baseline to 90% peak (Time-to-90%peak, D), time from peak to 90% relaxation (Time-to-90%relaxztion, E), velocity of systole ($V_{systolic}$, F), and velocity of diastole ($V_{diastolic}$, G). (**H**) Transmission electron microscopy depicting intracellular sarcomere and mitochondrial structures in ventricular heart tissues from 75%KD and WT mice. Arrows highlight the adherens junction structures. **P*<0.05, ***P*<0.01 versus WT group. Statistical significance of differences was assessed by unpaired two-tailed Student *t*-tests.

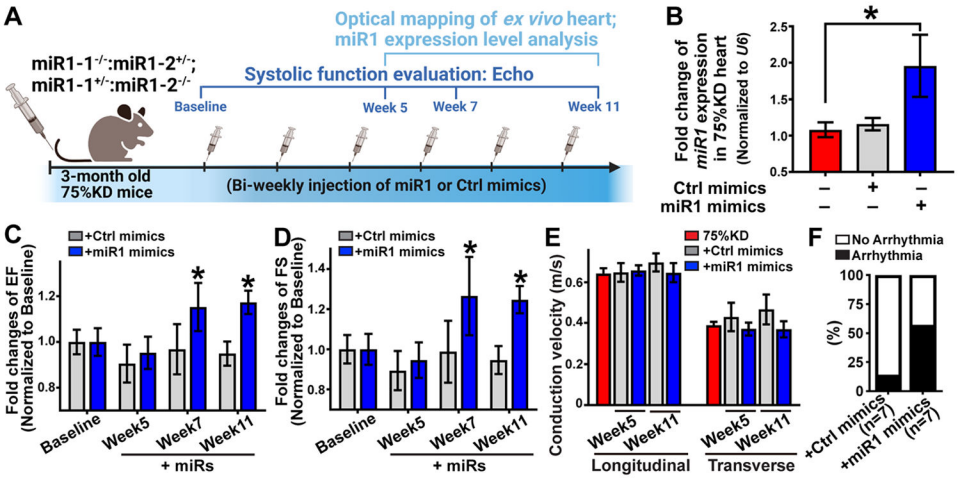

Figure 7.

Effects of miR1 restoration on 75%KD hearts. (**A**) Schematic representation of the rescue experiment for 75%KD heart through miR administration via intravenous tail vein injections. (**B**) qPCR analysis illustrating the significant increase of miR1 expression in 75%KD hearts (n=4), following tail vein injection of miR1 mimics. Expressions levels were normalized to *U6* RNA. (**C-D**) Echocardiography analysis demonstrating the enhanced ejection fraction (C) and fractional shortening (D) of 75%KD mice at Week 7 and Week 11 (n=4), compared to the control mimic group (n=4). (**E**) Optical mapping of *ex vivo* hearts showing no significant improvement in conduction velocity with miR1 administration in 75%KD animals at week 5 (n=3) and week 11 (n=4). (**F**) Programmed electric stimulation assays revealing no improvement in arrhythmia inducibility of 75%KD heart following miR1 administration. **P*<0.05 versus control mimics or indicated group. Statistical significance of differences was assessed by unpaired two-tailed Student *t*-tests.